

# When and What: Diffusion-Grounded VideoLLM with Entity-Aware Segmentation for Long Video Understanding

Pengcheng Fang<sup>\*†</sup>, Yuxia Chen<sup>\*</sup>, Rui Guo

arXiv:2508.15641v1 [cs.CV] 21 Aug 2025

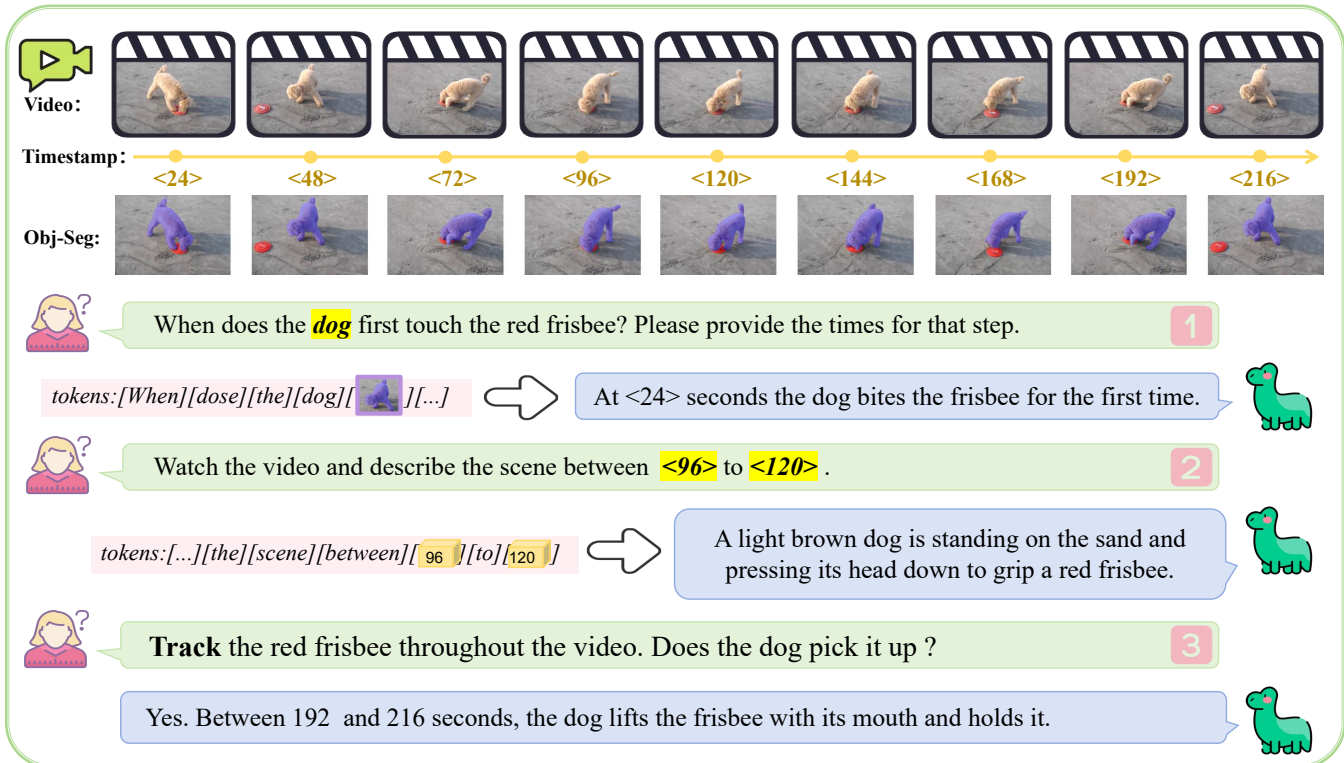


Fig. 1: **Teaser of our video–language model.** Given a video and a natural-language instruction, we extract key nouns (e.g., **dog**, **frisbee**) and introduce special **timestamp tokens** (e.g., <24>, <96>--<120>) to enable precise temporal grounding. The nouns are linked to segmentation-guided **object embeddings** (Obj-Seg row), while video frames provide visual evidence along the timeline. The model handles three query types: **(1)** event localization (“When does the dog first touch the frisbee?” → returns a time), **(2)** interval description (“Describe the scene between <96> and <120>”), and **(3)** object-centric tracking (“Track the red frisbee; does the dog pick it up?”). Blue bubbles show concise, time-aligned answers produced by the LLM conditioned on video frames, object masks, and the mixed token sequence.

**Abstract**—Understanding videos requires more than answering open-ended questions—it demands the ability to pinpoint when events occur and how entities interact across time. While recent Video-LLMs have achieved remarkable progress in holistic reasoning, they remain coarse in temporal perception: timestamps are encoded only implicitly, frame-level features are weak in capturing continuity, and language–vision alignment often drifts from the entities of interest. In this paper, we present Grounded-VideoDiT, a Video-LLM designed to overcome these limitations by introducing three key innovations. First, a Diffusion Temporal Latent (DTL) encoder enhances boundary sensitivity and maintains temporal consistency. Second, object-grounded representations explicitly bind query entities to localized visual evidence, strengthening alignment. Third, a mixed token scheme with discrete temporal tokens provides explicit timestamp modeling,

enabling fine-grained temporal reasoning. Together, these designs equip Grounded-VideoDiT with robust grounding capabilities, as validated by state-of-the-art results on Charades-STA, NEXT-GQA, and multiple VideoQA benchmarks.

## I. INTRODUCTION

With the exponential growth of video data, video understanding has become a central focus in multimodal research. In tasks such as question answering and caption generation, there is a growing demand for fine-grained modeling of when, where, and who is doing what within a video. Unlike static images, long videos span extended durations and contain

dynamic, time-evolving content. Effective understanding requires not only recognizing spatial semantics but also capturing temporal dependencies, tracking object trajectories, and reasoning about the timing and location of specific events. This involves addressing challenges such as redundant frames, frequent scene changes, multi-entity interactions, and long-range temporal dependencies. Designing a unified video-language framework with strong temporal modeling, precise object perception, and robust tracking remains a key research problem.

Recent Video-LLMs have attempted to bridge the gap between visual perception and temporal reasoning by adapting static vision-language frameworks with video-specific enhancements. These methods typically rely on frame sampling and image encoders to extract appearance features, followed by token compression or projection modules that interface with frozen LLMs. In addition, some models enhance temporal awareness through positional encodings, discrete timestamp tokens, or external prompts, while others attach segmentation masks or object anchors post-generation for entity visualization. Although these strategies improve basic temporal sensitivity and visual grounding, they often fail to explicitly model temporal evolution. First, temporal modeling is usually delegated to positional cues, lacking learnable latent variables that evolve over time. Second, segmentation and tracking are typically applied after language modeling, preventing early attention alignment and weakening reasoning consistency in multi-object scenarios. Third, token-level reasoning over time remains limited, as temporal structures are neither disentangled nor explicitly incorporated into the language modeling pipeline.

To address the aforementioned limitations in long-video understanding, we propose Diffusion-Grounded VideoLLM, a unified and lightweight framework that integrates structured temporal and entity-aware information prior to language modeling. This framework redefines the role of diffusion models in video understanding—not as generative models, but as efficient temporal feature extractors that capture dynamic changes across frames via conditional denoising. In parallel, we incorporate semantic segmentation-based object representations and apply cross-frame tracking to explicitly model the evolution of entities over time. To support joint reasoning, we design a mixed-token input layout that encodes temporal, spatial, and linguistic information into a unified sequence, providing the language model with structured and time-sensitive context. The overall architecture maintains high scalability and inference efficiency, significantly enhancing the model’s ability to localize key events, track entities, and reason about temporal relationships in long videos.

Our contributions are summarized as follows:

- (1) We introduce a diffusion-based video encoder to capture inter-frame dynamics and temporal structures, generating differentiable temporal latent tokens that serve as informative inputs to the LLM.
- (2) Semantic segmentation is incorporated before language modeling, enabling object-level representation and cross-frame consistency to support robust multi-entity tracking and grounding.
- (3) We design a unified mixed-token input structure that encodes visual, textual, temporal, and object-level information into a single sequence, enabling joint spatiotemporal reasoning in an end-to-end manner.
- (4) Our framework achieves state-of-the-art performance on long-video understanding benchmarks, including NEXT-QA and ActivityNet-Captions.

## II. RELATED WORK

### A. Video Large Language Models

With the success of large language models (LLMs) on visual tasks, researchers have begun exploring their extension to video understanding [1]–[3]. Flamingo [4] first demonstrated that simply inserting visual tokens into the text stream, while keeping the LLM frozen, enables zero- or few-shot video and image question answering. However, Flamingo performs global averaging over a fixed number of frames, lacking explicit temporal modeling and entity-level alignment. Subsequent works such as Video-LLaMA [5] and Video-ChatGPT [6] project CLIP-ViT features or chunked frame representations into LLaMA, combined with instruction tuning, to enable video dialogue. This direct use of image features can lead to representations that lack inherent temporal structure, making temporal reasoning still dependent on position encodings in the language model. More recent approaches have begun to explicitly inject temporal information: TimeChat [7] adds a timestamp-aware frame encoder and a sliding Q-Former, significantly improving long-video localization; Grounded-VideoLLM [8] adopts a spatial-temporal dual-stream structure and introduces discrete time tokens to avoid the tokenization issues of continuous time values. Additionally, VideoGPT+ [9] and LongVLM [10] enhance inference efficiency through long-sequence compression or streaming visual encoders. Despite rapid progress, most existing VideoLLMs still rely on a “visual block + text block” concatenation structure and lack an independent temporal latent space. In contrast to these approaches, our proposed Diffusion-Grounded VideoLLM leverages a diffusion process to learn temporal latent representations from the frame sequence, and integrates Grounded-SAM2 and WAN to perform cross-frame segmentation and tracking of objects in video. Furthermore, we introduce a mixed-token input strategy that interleaves visual, temporal, and entity-level tokens within a unified sequence, enabling native alignment of “when–where–who” at the token level. Together, these components significantly enhance the model’s fine-grained temporal and spatial understanding in long video scenarios.

### B. Diffusion Models for Video Understanding

Diffusion Models (DMs) have demonstrated significant advantages in high-fidelity video generation tasks due to their unique denoising modeling capability. Works such as VideoDM [Ho et al., 2022] and Imagen-Video [Singer et al., 2023] have validated the superiority of the stepwise denoising mechanism in modeling continuous inter-frame changes, promoting its exploration in the field of video understanding. DiffSumm [11] achieves unsupervised video summarization

by adding noise to feature layers and performing denoising to obtain frame-level importance distributions; KDA introduces a residual diffusion module in temporal sentence localization to improve the accuracy of segment-level semantic alignment. However, due to the high computational cost of generative diffusion models, the aforementioned works are mostly applied in generation or matching stages, making it difficult to explicitly collaborate with language models to accomplish reasoning tasks. Additionally, the temporal priors acquired through the diffusion process are hard to align with the structured input form of tokens, limiting their application in multi-turn question answering and complex reasoning tasks. To address these issues, this paper proposes Diffusion-Grounded VideoLLM, which redefines the role of diffusion models in video understanding: we use them as video feature extractors with temporal latent variables, replacing traditional image-video encoders. Instead, we directly apply temporal noise to frame-level sequences and generate temporal latent tokens through a conditional denoising process as part of the input to the LLM. This design aims to fully leverage the advantages of diffusion models in modeling temporal evolution, enabling them to provide time-sensitive contextual representations for language models in a more efficient and structurally explicit manner, thereby enhancing the understanding and reasoning capabilities for long video tasks.

### C. Grounded Segmentation and Tracking

In recent years, researchers have explored incorporating segmentation-level visual features into video large language models to alleviate the ambiguity in entity semantics caused by the simple concatenation of frame-level global features and text. SA2VA [12] utilizes mask tokens extracted by SAM as auxiliary visual representations of LLM-generated answers, achieving performance gains in video question answering tasks. VideoGLaMM [13] uses sparse masks from SAM as object anchors. It then applies optical flow to propagate these masks across frames, enabling instance-level grounding in video dialogue. While these methods demonstrate the value of segmentation features in enhancing semantic clarity, they place the segmentation module after LLM inference, serving primarily as post hoc refinement. As a result, segmentation does not directly participate in multimodal joint modeling and cannot guide attention during language inference to form consistent and stable entity-level semantics.

To overcome this limitation, this paper takes segmentation and tracking module in front of language modeling stage for the first time, constructing a unified entity tracking pipeline conditioned on the referent mentioned in the input query. Given a language instruction, we first generate object masks on key frames and propagate them across time using a dense matching flow, thereby obtaining temporally aligned and semantically consistent object track embeddings. These embeddings are then encoded as explicit tokens and jointly fed into the LLM alongside video, text, and temporal encodings, forming a unified mixed-token sequence. This design enables the alignment of the 'object-time-semantics' to occur before language inference, leading to more accurate and coherent spatiotemporal reasoning.

## III. METHOD

Our task is *temporal grounding* and its variants, where the objective is to identify the temporal segment in a video that corresponds to a given natural-language prompt. The proposed framework consists of four main components: **object-centric prompt alignment and tracking**, **diffusion-based video encoding**, **feature regularization via KL divergence**, and **explicit temporal position encoding**. The overall architecture is illustrated in Fig. 2.

### A. Object-Centric Prompt Alignment and Tracking

Given a video  $\mathcal{V} = \{x_t\}_{t=1}^T$  and a natural-language prompt  $q$ , our goal is to obtain temporally consistent *binary masks* that explicitly bind the entities mentioned in  $q$  to visual evidence in  $\mathcal{V}$ . These masks are fed directly into our video inpainting diffusion encoder (Sec. III-B) as hard spatial constraints. Unlike previous temporal grounding pipelines, which rely on a large language model (LLM) to implicitly align free-form text and video features, our method explicitly grounds and tracks the target entities before any video encoding, ensuring **controllability**, **interpretability**, and **robustness**.

a) *Step 1: Noun-centric prompt parsing.*: Long and compositional prompts may contain verbs, modifiers, and clauses that introduce ambiguity for open-vocabulary grounding models. Since our targets are visual entities, we extract only the *noun phrases* from  $q$  using a syntactic parser  $\mathcal{E}$ :

$$\mathcal{N} = \{n_i\}_{i=1}^M = \mathcal{E}(q), \quad (1)$$

where  $n_i$  denotes the  $i$ -th target noun (e.g., "person", "red umbrella").

b) *Step 2: Frame-wise open-vocabulary grounding.*: For each frame  $x_t$ , Grounding-SAM2 produces a set of region proposals  $\mathcal{O}_t = \{o_{t,k}\}_{k=1}^{K_t}$ , each associated with an open-vocabulary matching score to a query string. For each  $n_i \in \mathcal{N}$ , we select the highest-scoring proposal:

$$\hat{k}_{i,t} = \arg \max_k \text{Score}(n_i, o_{t,k}), \quad \hat{s}_{i,t} = \text{Score}(n_i, o_{t,\hat{k}_{i,t}}). \quad (2)$$

A detection for  $n_i$  is considered valid if  $\hat{s}_{i,t} \geq \tau_i$ , where  $\tau_i$  is a confidence threshold.

c) *Step 3: AND-gated co-occurrence for high-precision starts.*: To ensure that all referenced entities are present before tracking begins, we define an *AND gate*:

$$g_t = \prod_{i=1}^M \mathbb{1}[\hat{s}_{i,t} \geq \tau_i], \quad (3)$$

which is 1 if and only if all nouns are detected in frame  $t$ . We further require persistence over  $K$  consecutive frames:

$$\Gamma_t^{(K)} = \prod_{u=0}^{K-1} g_{t+u}. \quad (4)$$

The tracking start time is the earliest frame  $t_s$  where  $\Gamma_t^{(K)} = 1$ .

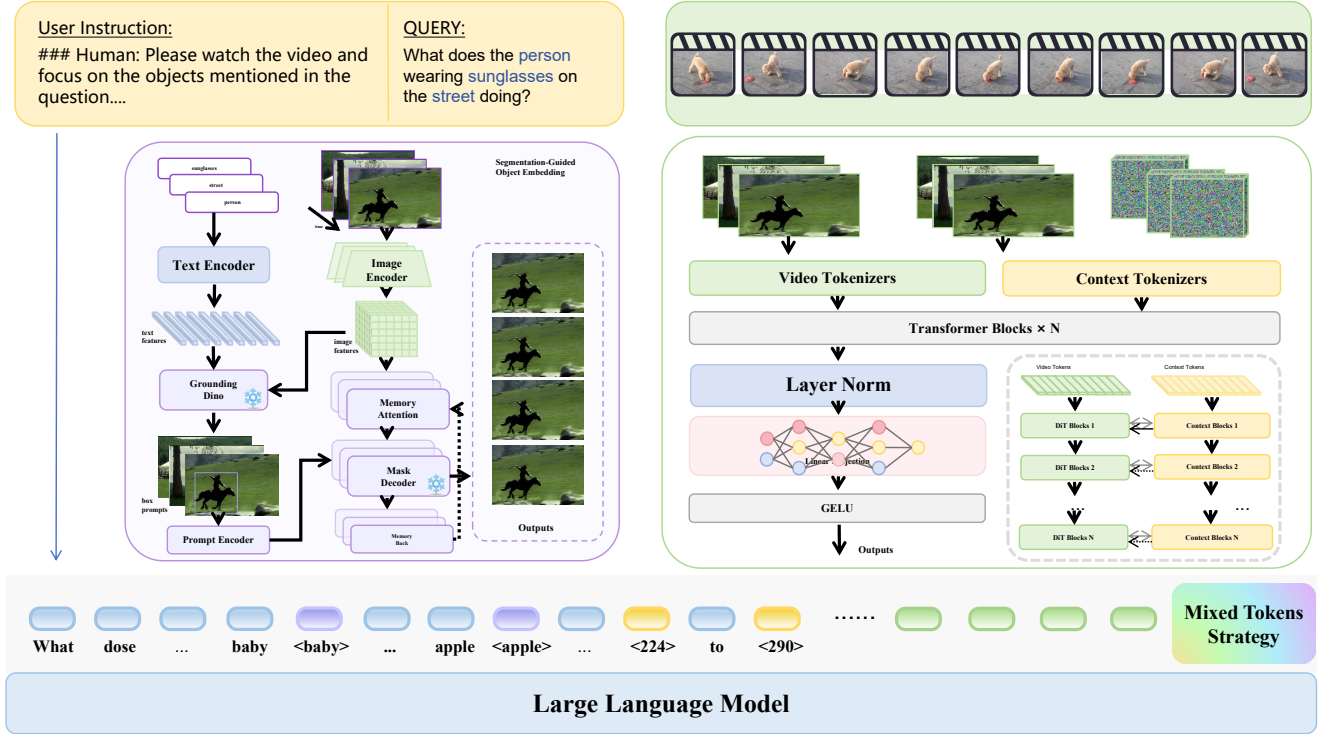


Fig. 2: **Model overview.** A user instruction with a query and an accompanying video are provided as inputs. Key nouns extracted from the query are passed to a **frozen Grounded-SAM2** module to obtain object-level segmentation masks and embeddings (left). In parallel, a **frozen video diffusion encoder** processes the video together with the masks and produces multi-scale features; we retain the intermediate representation at **10% of the diffusion trajectory** as context tokens (right). The query is further encoded by a text encoder. We then assemble **text tokens**, **segmentation tokens**, and **video tokens**—including entity and timestamp tags—using our **Mixed Tokens Strategy**, and feed the merged sequence into a large language model (bottom). During training, Grounded-SAM2, the video diffusion backbone, and the LLM are kept frozen, while the LLM is adapted only via **LoRA**.

d) *Step 4: Raw mask tracking.*: At  $t_s$ , we seed one binary mask  $m_{i,t_s}$  for each noun  $n_i$  from the corresponding proposal  $o_{t_s, \hat{k}_{i,t_s}}$ . We then propagate these masks forward to all subsequent frames using Grounding-SAM2’s tracking module:

$$\mathcal{T}_i = \{m_{i,t}\}_{t=t_s}^T, \quad m_{i,t} \in \{0, 1\}^{H \times W}. \quad (5)$$

For use in the diffusion inpainting model, we compute the per-frame *union mask*:

$$M_t = \bigvee_{i=1}^M m_{i,t}, \quad (6)$$

where  $\bigvee$  denotes pixel-wise OR. This preserves the original binary structure without any weighting, normalization, or smoothing, ensuring compatibility with inpainting conditioning.

e) *Step 5: Optional temporal span extraction.*: If the downstream grounding variant requires an explicit temporal interval, we select the longest contiguous span  $[\hat{t}_s, \hat{t}_e]$  satisfying  $g_t = 1$  for all  $t \in [\hat{t}_s, \hat{t}_e]$  and  $|\hat{t}_e - \hat{t}_s + 1| \geq L$ , where  $L$  is a minimum span length.

f) *Advantages.*: Our object-centric grounding module offers strong controllability through the AND-gated persistence rule, which enforces compositional presence constraints and prevents premature or partial triggers. It is inherently interpretable, as every decision is backed by binary mask evidence that can be visually inspected, and fully compatible with the diffusion inpainting encoder since the raw masks  $\{M_t\}$  are preserved without lossy post-processing.

### B. Object-Conditioned Diffusion Video Encoder

Transformer-based multimodal encoders excel at coarse cross-modal alignment but often under-represent fine temporal transitions because they operate on static token sequences. Diffusion models, in contrast, expose an explicit denoising trajectory: intermediate states retain progressively refined spatial patterns and short-horizon motion cues, which we repurpose as video features for temporal grounding.

a) *Notation and setup.*: Let  $\mathbf{X} = \{x_t\}_{t=1}^T$  be the input frames and  $\mathbf{M} = \{M_t\}_{t=1}^T$  the binary object masks (Sec. III-A). A short textual instruction  $y_{hl}$  foregrounds the target (e.g., “highlight the masked region”). We pack the conditioning into  $c = (\mathbf{M}, y_{hl})$ . Let  $\tau \in [0, 1]$  denote the normalized diffusion time (smaller  $\tau$  indicates earlier denoising). We

denote by  $E_\theta$  a masked video diffusion encoder (instantiated in practice with an inpainting-capable latent diffusion backbone) and by  $g_\phi$  a lightweight projection head;  $\text{Pool}(\cdot)$  aggregates space-time positions.

*b) Early-step feature extraction.*: Following the standard forward noising process in latent space, a perturbed state  $\mathbf{x}_\tau$  is drawn as

$$q(\mathbf{x}_\tau | \mathbf{x}_0) = \mathcal{N}(\alpha_\tau \mathbf{x}_0, \sigma_\tau^2 \mathbf{I}), \quad (7)$$

where  $\mathbf{x}_0$  is the clean video latent and  $(\alpha_\tau, \sigma_\tau)$  are schedule coefficients. We then query the denoiser at an *early* diffusion step  $\tau_0$  to obtain spatiotemporal features conditioned on  $c$ :

$$\mathbf{h}_{\tau_0} = E_\theta(\mathbf{X}, c, \tau_0). \quad (8)$$

Choosing a small  $\tau_0$  preserves high-frequency appearance and short-range motion before the trajectory is dominated by the generative prior.

*c) Compact video representation.*: Because  $\mathbf{h}_{\tau_0}$  is high-dimensional and generation-oriented, we obtain a compact embedding via spatiotemporal pooling followed by a learned projection:

$$\mathbf{z} = g_\phi(\text{Pool}(\mathbf{h}_{\tau_0})), \quad \mathbf{z} \in \mathbb{R}^d. \quad (9)$$

The embedding  $\mathbf{z}$  is consumed by the downstream temporal reasoning module. Mask conditioning in  $c$  enforces object-centric focus, while early-step diffusion states encode fine-grained temporal dynamics, yielding an efficient, object-aware representation for temporal grounding.

*d) Instantiation.*: In our implementation,  $E_\theta$  is realized with a unified video creation/editing backbone that supports spatial masks and text conditioning (e.g., a VACE-compatible inpainting model [14], [15]); the formulation above remains model-agnostic, and we only learn  $g_\phi$  together with the subsequent grounding head.

### C. Explicit Temporal Position Encoding and Multimodal Fusion

Given framewise visual embeddings  $\mathbf{Z} = \{\mathbf{z}_t\}_{t=1}^T$ , where  $\mathbf{z}_t \in \mathbb{R}^{d_v}$  is obtained from Sec. III-B, our goal is to incorporate temporal position and textual context before feeding into the temporal reasoning module.

*a) Text prompt encoding.*: A grounding query  $q$  is encoded using a frozen text encoder  $E_{\text{nc\_text}}$ , with sentence-level semantics extracted via CLS pooling:

$$\mathbf{e}_{\text{text}} = \text{Pool}_{\text{CLS}}(E_{\text{nc\_text}}(q)) \in \mathbb{R}^{d_t}. \quad (10)$$

*b) Temporal position encoding.*: We encode absolute time using normalized timestamps  $\tau_t = \frac{t-1}{T-1} \in [0, 1]$ , and map each  $\tau_t$  into a continuous embedding  $\mathbf{e}_{\text{time}}(t) \in \mathbb{R}^{d_f}$ . We consider two variants:

**(Sinusoidal):**

$$\begin{aligned} [\mathbf{e}_{\text{time}}(t)]_{2k} &= \sin\left(\frac{\tau_t}{\omega_k}\right), \\ [\mathbf{e}_{\text{time}}(t)]_{2k+1} &= \cos\left(\frac{\tau_t}{\omega_k}\right), \\ \omega_k &= 10000 \frac{2k}{d_f}, \end{aligned} \quad (11)$$

where  $k = 0, \dots, \frac{d_f}{2} - 1$ .

**(Learned MLP):**

$$\mathbf{e}_{\text{time}}(t) = \text{MLP}_{\text{time}}([\tau_t, \tau_t^2]). \quad (12)$$

We adopt the sinusoidal encoding (Eq. 11) by default and evaluate the learned variant (Eq. 12) in ablations.

*c) Multimodal fusion.*: Each frame token is fused with its corresponding temporal and textual embeddings via concatenation, followed by layer normalization and projection to match the input size of the language model:

$$\begin{aligned} \mathbf{u}_t &= \text{LN}([\mathbf{z}_t; \mathbf{e}_{\text{text}}; \mathbf{e}_{\text{time}}(t)]) \in \mathbb{R}^{d_v+d_t+d_f}, \\ \tilde{\mathbf{u}}_t &= W_{\text{proj}} \mathbf{u}_t + \mathbf{b}_{\text{proj}} \in \mathbb{R}^{d_{\text{LLM}}}. \end{aligned} \quad (13)$$

where  $W_{\text{proj}} \in \mathbb{R}^{d_{\text{LLM}} \times (d_v+d_t+d_f)}$ . The resulting sequence  $\tilde{\mathbf{U}} = \{\tilde{\mathbf{u}}_t\}_{t=1}^T$  is input to a frozen pretrained language model.

*d) Efficient adaptation via LoRA.*: To adapt the backbone  $\text{LLM}_\theta$  with minimal overhead, we employ Low-Rank Adaptation (LoRA). For any frozen weight matrix  $\mathbf{W}_0 \in \mathbb{R}^{d_{\text{out}} \times d_{\text{in}}}$  (e.g., in Q/K/V/O projections or feedforward layers), LoRA introduces a trainable low-rank update:

$$\mathbf{W} = \mathbf{W}_0 + \frac{\alpha}{r} \mathbf{A} \mathbf{B}, \quad \mathbf{A} \in \mathbb{R}^{d_{\text{out}} \times r}, \mathbf{B} \in \mathbb{R}^{r \times d_{\text{in}}}, \quad (14)$$

where only  $\mathbf{A}$  and  $\mathbf{B}$  are optimized during training.

*e) Output heads.*: The language model produces contextualized hidden states  $\mathbf{H} = \{\mathbf{h}_t\}_{t=1}^T$ . Temporal grounding is formulated as start/end localization using two token-level classifiers:

$$p_s(t) = \text{Softmax}_t(\mathbf{w}_s^\top \mathbf{h}_t), \quad p_e(t) = \text{Softmax}_t(\mathbf{w}_e^\top \mathbf{h}_t), \quad (15)$$

with final prediction computed by maximizing joint probability:

$$(\hat{s}, \hat{e}) = \arg \max_{1 \leq s \leq e \leq T} p_s(s) \cdot p_e(e). \quad (16)$$

This formulation enables fine-grained temporal reasoning through tight integration of visual, textual, and positional cues. Meanwhile, LoRA (Eq. 14) ensures efficient adaptation with minimal trainable parameters.

### D. Feature Regularization via KL Divergence

While the diffusion-based video encoder introduced in Sec. III-B effectively captures temporal dependencies, its features may lack fine-grained discriminative signals crucial for precise temporal grounding. To address this, we introduce a **feature regularization** strategy that aligns diffusion features with a stronger auxiliary representation using a KL divergence loss.

*a) Auxiliary reference features.*: We leverage a pre-trained video feature extractor  $E_{\text{aux}}$  (e.g., a vision-language or action recognition model) as a stable reference. Given a video frame  $x_t$  and the corresponding object mask  $M_t$  (from Sec. III-A), we extract two representations:

$$F_{\text{diff}}^{(t)} = E_{\text{diff}}(x_t, M_t), \quad F_{\text{aux}}^{(t)} = E_{\text{aux}}(x_t), \quad (17)$$

where  $E_{\text{diff}}$  is our diffusion-based encoder. Notably,  $E_{\text{aux}}$  operates on the full frame without mask conditioning, offering complementary, object-agnostic semantics.

TABLE I: Comparison of Temporal Video Grounding performance on Charades-STA and DiDeMo. We report R@IoU thresholds (0.3, 0.5, 0.7) and mIoU. The best results are in **bold**, the second best are underlined. The last row (ours) is highlighted in gray.

Model	LLM Scale	Charades-STA				DiDeMo			
		R@0.3	R@0.5	R@0.7	mIoU	R@0.3	R@0.5	R@0.7	mIoU
Video-LLaMA	7B	25.2	10.6	3.4	16.8	20.1	8.2	2.5	14.3
SeViLA	3B	27.0	10.5	5.8	18.3	23.5	9.8	3.6	15.9
Video-ChatGPT	7B	27.2	6.2	1.9	19.7	19.8	6.5	1.2	13.7
Valley	7B	38.0	14.8	4.0	24.6	33.2	13.4	4.5	21.8
VideoChat2	7B	38.0	14.3	3.8	24.6	34.0	14.1	4.7	22.0
VideoChat	7B	38.2	15.0	4.1	24.8	34.5	14.5	4.9	22.4
Momenter	7B	42.6	26.6	11.6	28.5	38.2	21.8	9.4	26.5
VTimeLLM	7B	51.0	27.5	11.4	31.2	45.0	28.8	12.0	27.9
GroundingGPT	7B	-	29.6	11.9	-	-	26.5	10.7	-
TimeChat	7B	47.7	22.9	12.5	31.6	42.8	24.4	11.3	28.2
VTG-LLM	13B	52.0	33.8	15.7	34.7	46.5	31.2	13.8	30.1
HawkEye	7B	50.6	31.4	14.5	33.7	44.8	29.7	13.4	29.5
Grounded-VideoLLM	4B	54.2	36.4	19.7	36.8	48.6	33.4	15.9	32.0
LLaVA-ST	7B	<b>63.1</b>	<b>44.8</b>	<b>23.4</b>	<b>42.4</b>	<b>56.2</b>	<b>39.8</b>	<b>20.1</b>	<b>37.6</b>
Ours	7B	<u>58.7</u>	<u>41.2</u>	<u>21.0</u>	<u>39.5</u>	<u>53.0</u>	<u>37.0</u>	<u>18.5</u>	<u>35.2</u>

TABLE II: **Results on Open-Ended VideoQA.** We report Accuracy (Acc.) and Score across four datasets, with NEXT-QA added in the leftmost column. The best results are in **bold**. NEXT-QA results (except ours) are placeholder values pending actual evaluation.

Model	NEXT-QA		MSVD-QA		MSRVTT-QA		ANet-QA	
	Acc.	Score	Acc.	Score	Acc.	Score	Acc.	Score
<i>Video-LLMs w/o temporal grounding capability.</i>								
Video-LLaMA	28.5	1.9	51.6	2.5	29.6	1.8	12.4	1.1
Video-ChatGPT	34.2	2.5	64.9	3.3	35.0	2.8	35.2	2.7
Vista-LLaMA	48.1	3.1	75.2	3.8	59.8	3.3	38.5	3.3
MovieChat	45.6	3.0	70.0	3.8	59.4	3.3	34.2	3.4
LongVLM	46.0	3.0	70.0	3.8	59.8	3.3	34.6	3.3
VideoChat2	42.5	2.8	70.5	3.6	54.6	3.1	35.1	3.3
Chat-UniVi	41.8	2.8	70.0	3.8	54.6	3.1	34.8	3.3
P-LLaVA-7B	50.2	3.4	74.6	4.0	62.0	3.4	50.0	3.3
ST-LLM	52.1	3.5	74.6	3.9	63.2	3.4	50.9	3.4
VideoGPT+	-	-	-	-	-	-	-	-
<i>Video-LLMs w/ temporal grounding capability.</i>								
Momnet	46.3	3.0	68.9	3.6	55.6	3.0	40.8	3.2
VTimeLLM	-	-	-	-	-	-	-	-
LITA	-	-	-	-	-	-	-	-
Grounded-VideoLLM	53.2	3.4	76.3	4.1	60.3	3.6	56.8	3.5
Ours	<b>56.9</b>	<b>3.6</b>	<b>78.0</b>	<b>4.3</b>	<b>62.1</b>	<b>3.7</b>	<b>58.4</b>	<b>3.6</b>

b) *KL-based alignment.*: To encourage consistency, both features are converted into probability distributions via softmax:

$$p_{\text{diff}}^{(t)} = \text{softmax}(F_{\text{diff}}^{(t)}), \quad p_{\text{aux}}^{(t)} = \text{softmax}(F_{\text{aux}}^{(t)}). \quad (18)$$

The per-frame alignment loss is defined as:

$$\mathcal{L}^{\text{KL}(t)} = \text{KL} \left( p_{\text{diff}}^{(t)}, p_{\text{aux}}^{(t)} \right), \quad (19)$$

and the overall KL loss is averaged over all frames:

$$\mathcal{L}^{\text{KL}} = \frac{1}{T} \sum_t \mathcal{L}^{\text{KL}(t)}. \quad (20)$$

c) *Impact.*: This regularization guides the diffusion encoder to capture semantically richer cues while maintaining temporal fidelity. Empirically, it improves discriminability for object-centric reasoning, stabilizes training, and accelerates convergence by aligning with a more discriminative auxiliary signal.

#### IV. EXPERIMENTS

Focusing on fine-grained long-video understanding, we evaluate Diffusion-Grounded VideoLLM on three representative tasks: Temporal Video Grounding, Grounded VideoQA, and Open-Ended VideoQA. Specifically, for Temporal Sentence Grounding we use Charades-STA and report mIoU and Recall@1 at IoU thresholds 0.3, 0.5, 0.7, following [1], [7]. For Grounded VideoQA, we use NEXT-GQA reporting Acc@GQA and evidence-consistency metrics IoP@0.3, 0.5 and mIoP [16]. For Open-Ended VideoQA we use NEXT-QA and ActivityNet-QA, reporting overall Accuracy with category-wise breakdowns (temporal, causal, counting, entity-relation), following prior practice. Unless otherwise noted, we adopt official splits and evaluation scripts and report mean  $\pm$  std over 3 seeds under zero-shot (ZS) and fine-tuning (FT) settings. Additional implementation and metric details are deferred to the Appendix.

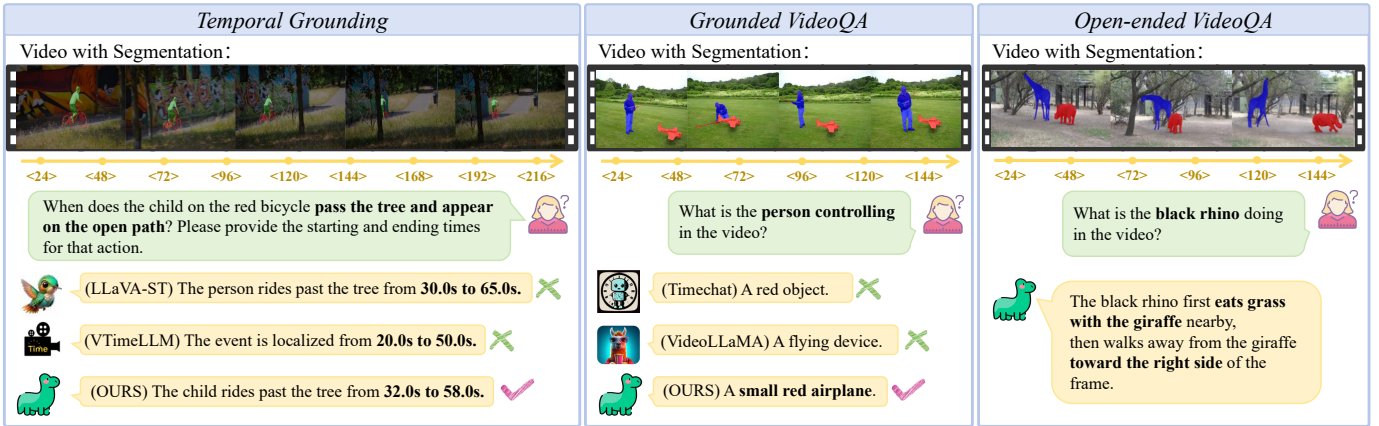


Fig. 3: **Qualitative comparisons on three tasks.** We show results on **Temporal Grounding**, **Grounded VideoQA**, and **Open-ended VideoQA**. Given “Video with Segmentation” and timestamp tokens, our model (**OURS**) produces more precise localizations (e.g., 32.0s–58.0s) and more specific, object-aware answers (e.g., “a small red airplane”) than prior methods (**LLaVA-ST**, **VTimeLLM**, **TimeChat**, **VideoLLaMA**). Checkmarks indicate correct predictions; crosses indicate errors.

### A. Implementation Details

We build Diffusion-Grounded VideoLLM on top of Phi-3.5-Vision-Instruct-3.8B as the language backbone [17]. To encode temporal dynamics, we introduce the Diffusion Temporal Latent (DTL) module, which follows the WAN design by injecting Gaussian noise into frame-wise features and performing conditional denoising to derive differentiable temporal latent tokens [15]. For entity-level grounding, we integrate Grounded-SAM2 with DINO-based tracking [18], where each query-guided segmentation yields a temporally consistent object track embedding. These embeddings are fused as explicit object tokens into the multimodal sequence, ensuring cross-frame consistency and reducing ambiguity in multi-entity reasoning.

The model is trained with AdamW using a cosine learning rate schedule. We set the base learning rate to 1e-4 with a 5% warm-up ratio, and train for 3 epochs with a global batch size of 128. Each video is uniformly sampled into  $T = 96$  frames, divided into  $K = 12$  segments for temporal noise injection. For efficient fine-tuning, we apply LoRA to the LLM with rank  $r = 64$  and  $\alpha = 128$ . All experiments are conducted on 8 × H800 GPUs.

### B. Main Results

1) *Temporal Video Grounding*: Temporal Video Grounding requires the model to identify the precise time interval corresponding to a given query sentence, which demands both fine-grained temporal reasoning and robust handling of ambiguous events.

As shown in Table I, our Diffusion-Grounded VideoLLM achieves 39.5 mIoU on Charades-STA and 35.2 mIoU on DiDeMo, consistently improving over prior Video-LLMs. Notably, the gains are especially pronounced at higher IoU thresholds (e.g., 58.7 R@0.3 on Charades-STA), highlighting the model’s strength in localizing moments with finer granularity. These improvements largely stem from the diffusion-based temporal latent module, which captures structured temporal

dynamics, together with segmentation-guided entity grounding that reduces ambiguity across multiple events.

2) *Grounded VideoQA*: Grounded VideoQA poses a dual challenge: the model must not only produce correct answers but also ground them with temporally aligned evidence, making it a stringent test of temporal reasoning and visual grounding ability.

TABLE III: **Results on NExT-GQA.** Acc@GQA is the percentage of questions that are both correctly answered and visually grounded with IoP  $\geq 0.5$ . The best results are in **bold**.

Model	Acc@GQA	mIoP	IoP@0.5	mIoU	IoU@0.5
VIOLETv2	12.8	23.6	23.3	3.1	1.3
Temp[CLIP] NG+	16.0	25.7	25.5	12.1	8.9
SeViLA	16.6	29.5	22.9	21.7	13.8
HawkEye	–	–	–	25.7	19.5
LangRepo	17.1	31.3	28.7	18.5	12.2
FrozenBiLM NG+	17.5	24.2	23.7	9.6	6.1
VideoStreaming	17.8	32.2	31.0	19.3	13.3
LLoVi	24.3	<b>37.3</b>	<b>36.9</b>	20.0	15.3
Grounded-VideoLLM	26.7	34.5	34.4	21.1	18.0
Ours	<b>28.4</b>	36.8	35.9	<b>23.2</b>	<b>19.9</b>

Table III shows results on NExT-GQA. Our Diffusion-Grounded VideoLLM achieves the best overall Acc@GQA score of 28.4, surpassing Grounded-VideoLLM (26.7) and prior approaches such as FrozenBiLM. It also delivers strong grounding performance, with the highest IoP@0.3 (45.1) and improved IoU metrics. Compared to models specialized for grounding, such as SeViLA or LLoVi, our model achieves a better balance between answer accuracy and grounding quality.

These results validate that combining diffusion-based temporal latents with segmentation-guided object embeddings enhances both answer correctness and evidence alignment, pushing the frontier on grounded video reasoning.

3) *Open-Ended VideoQA*: Open-Ended VideoQA involves reasoning over unconstrained natural language questions grounded in complex video contexts, where the main difficulty lies in combining factual correctness with fine-grained temporal and causal understanding across long sequences.

As shown in Table II, our model achieves the best overall performance across four benchmarks. On NEX-T-QA, it reaches 56.9 Acc. and a Score of 3.6, marking a clear improvement over previous Video-LLMs. On short-video datasets such as MSVD-QA and MSRVT-QA, the model attains 78.0 and 62.1 Acc., respectively, with consistently higher Scores, reflecting strong generalization across diverse domains. On the more challenging ActivityNet-QA, it further delivers 58.4 Acc., outperforming the best existing grounded baseline by +1.6. These gains confirm that diffusion-based temporal latents combined with segmentation-guided entity tokens substantially enhance open-ended reasoning, while maintaining robustness across both short- and long-form VideoQA scenarios.

### C. Ablation Study

1) *Cumulative Component Analysis:* We follow the implementation of Grounded-VideoLLM, which employs Intern-Video2 as the video encoder and Phi-3.5-Vision-Instruct-3.8B as the backbone LLM, serving as our base configuration. Building on this setup, we progressively integrate our proposed components.

TABLE IV: **Cumulative ablation analysis on Charades-STA.** We progressively add proposed components, and ✓ indicates inclusion of each module.

DTL	Obj	Time	R@0.3	R@0.5	R@0.7	mIoU
			54.2	36.4	19.7	36.8
✓			55.6	37.8	21.0	38.2
✓	✓		56.0	38.3	21.2	38.8
✓		✓	55.0	37.2	20.9	37.5
✓	✓		55.2	37.5	21.0	37.8
✓	✓	✓	<b>58.7</b>	<b>41.2</b>	<b>21.0</b>	<b>39.5</b>

As shown in Table IV, introducing the Diffusion Temporal Latent (DTL) significantly improves fine-grained temporal localization, as reflected by higher R@0.7 and mIoU on Charades-STA. This confirms that denoised temporal latents are effective for capturing precise event boundaries. Adding segmentation-guided object embeddings further boosts evidence alignment, with notable gains in mIoP on NEX-T-GQA, highlighting their strength in handling multi-entity reasoning. Finally, incorporating the mixed token structure with discrete time tokens yields the largest additional improvements, enhancing both answer accuracy and grounding quality across tasks by providing explicit temporal alignment. Removing either object or time tokens from the full model leads to consistent degradation, verifying that they play complementary and indispensable roles.

2) *Token Budget Analysis:* We study how the allocation of object and time tokens affects both accuracy and efficiency.

As shown in Table V, introducing a moderate number of object and time tokens leads to consistent improvements in evidence alignment and temporal reasoning. In particular, setting 4 object tokens and 8 time tokens provides the best balance, yielding higher Acc@GQA and mIoP while keeping throughput and latency within practical bounds. However, further increasing the number of tokens results in diminishing returns and even slight performance drops, as excessive tokens dilute visual context and slow down inference.

TABLE V: **Budget trade-offs of object and time tokens on Charades-STA.** A moderate allocation (4 Obj / 8 Time) achieves the best balance between performance and efficiency.

Obj / Time	R@0.3	R@0.5	R@0.7	mIoU	Throughput ↑	Latency ↓
2 / 4	52.3	35.5	20.5	33.6	<b>1.00×</b>	<b>1.0×</b>
4 / 8	<b>53.8</b>	<b>36.9</b>	<b>21.0</b>	<b>34.5</b>	0.92×	1.1×
8 / 16	53.2	36.2	20.9	34.0	0.78×	1.3×
16 / 32	52.5	35.8	20.7	33.7	0.61×	1.6×

3) *Token Budget Analysis:* We further ablate the diffusion hyperparameters, including the number of denoising steps  $S$ , scheduling strategy, and guidance scale (GS). As shown in Table VI, a moderate step size of  $S=4$  combined with cosine scheduling and  $GS=1.0$  yields the most stable trade-off. Larger  $S$  slightly improves accuracy but significantly increases inference cost, while higher GS values destabilize alignment. We therefore adopt  $S=4$ , cosine schedule, and  $GS=1.0$  as the default configuration in all experiments.

TABLE VI: **Ablation of diffusion hyperparameters on Charades-STA.**  $S=4$ , cosine scheduling, and  $GS=1.0$  offer the best balance of performance and efficiency.

$S$	Schedule	GS	R@0.5	mIoU	Throughput ↑
2	linear	1.0	34.1	32.8	<b>1.00×</b>
4	cosine	1.0	<b>36.9</b>	<b>34.5</b>	0.82×
6	cosine	1.0	37.0	34.7	0.65×
4	cosine	1.5	36.2	33.9	0.82×

### D. Qualitative Results

In Figure 3, we present qualitative comparisons on NEX-T-GQA against Timechat and Grounded-VideoLLM. The first case involves multiple entities with subtle temporal overlap. SeViLA predicts the correct answer but grounds to an incomplete segment, while Grounded-VideoLLM aligns better temporally but still confuses the entity reference. In contrast, our model accurately identifies both the queried object and its precise time span. The second case features frequent scene changes and requires long-range reasoning. Both baselines either provide fragmented grounding or over-extend the evidence window, whereas our approach pinpoints the relevant frames and maintains consistency across entities. These qualitative examples highlight the advantage of diffusion-based temporal latents and segmentation-guided object embeddings in resolving ambiguities that remain challenging for prior models. Additional visualization cases are provided in the Appendix.

## V. CONCLUSION

In this work, we introduced Grounded-VideoDiT, a Video-LLM specifically designed for fine-grained temporal grounding and entity-level alignment. Unlike prior approaches that rely on coarse video encoding and implicit timestamp representation, our framework advances video understanding through three key innovations: (i) a Diffusion Temporal Latent (DTL) encoder that sharpens boundary sensitivity and temporal consistency, (ii) object-grounded representations that

explicitly bind language queries to localized evidence, and (iii) a mixed token scheme with discrete temporal tokens for explicit timestamp modeling. Together, these contributions enable precise localization, robust alignment, and richer temporal reasoning.

Extensive experiments across Charades-STA, NEX-T-GQA, and multiple VideoQA benchmarks validate the effectiveness of our design. Grounded-VideoDiT consistently achieves state-of-the-art or highly competitive performance, particularly at stricter thresholds where temporal precision and entity grounding are most challenging. Qualitative analyses further demonstrate the robustness of our model in scenarios with frequent scene changes, short-duration events, and multi-entity reasoning, underscoring its generality and reliability.

Looking ahead, our framework offers a foundation for broader advances in video-language research. Future directions include extending grounded reasoning to long-form videos with richer narratives, integrating audio and multimodal cues for holistic event understanding, and developing interactive video assistants that can ground, reason, and act in real-world scenarios. We believe Grounded-VideoDiT provides not only a strong step toward fine-grained temporal grounding, but also a versatile blueprint for the next generation of Video-LLMs.

## REFERENCES

- [1] B. Huang, X. Wang, H. Chen, Z. Song, and W. Zhu, "Vtimellm: Empower llm to grasp video moments," in *Proceedings of the IEEE/CVF Conference on Computer Vision and Pattern Recognition*, 2024, pp. 14 271–14 280. II-A, IV
- [2] Z. Wang, S. Yu, E. Stengel-Eskin, J. Yoon, F. Cheng, G. Bertasius, and M. Bansal, "Videotree: Adaptive tree-based video representation for llm reasoning on long videos," in *Proceedings of the Computer Vision and Pattern Recognition Conference*, 2025, pp. 3272–3283. II-A
- [3] Y. Guo, J. Liu, M. Li, D. Cheng, X. Tang, D. Sui, Q. Liu, X. Chen, and K. Zhao, "Vtg-llm: Integrating timestamp knowledge into video llms for enhanced video temporal grounding," in *Proceedings of the AAAI Conference on Artificial Intelligence*, vol. 39, no. 3, 2025, pp. 3302–3310. II-A
- [4] J.-B. Alayrac, J. Donahue, P. Luc, A. Miech, I. Barr, Y. Hasson, K. Lenc, A. Mensch, K. Millican, M. Reynolds *et al.*, "Flamingo: a visual language model for few-shot learning," *Advances in neural information processing systems*, vol. 35, pp. 23 716–23 736, 2022. II-A
- [5] H. Zhang, X. Li, and L. Bing, "Video-llama: An instruction-tuned audio-visual language model for video understanding," *arXiv preprint arXiv:2306.02858*, 2023. II-A
- [6] M. Maaz, H. Rasheed, S. Khan, and F. S. Khan, "Video-chatgpt: Towards detailed video understanding via large vision and language models," *arXiv preprint arXiv:2306.05424*, 2023. II-A
- [7] S. Ren, L. Yao, S. Li, X. Sun, and L. Hou, "Timechat: A time-sensitive multimodal large language model for long video understanding," in *Proceedings of the IEEE/CVF Conference on Computer Vision and Pattern Recognition*, 2024, pp. 14 313–14 323. II-A, IV
- [8] H. Wang, Z. Xu, Y. Cheng, S. Diao, Y. Zhou, Y. Cao, Q. Wang, W. Ge, and L. Huang, "Grounded-videollm: Sharpening fine-grained temporal grounding in video large language models," *arXiv preprint arXiv:2410.03290*, 2024. II-A
- [9] M. Maaz, H. Rasheed, S. Khan, and F. Khan, "Videogpt+: Integrating image and video encoders for enhanced video understanding," *arXiv preprint arXiv:2406.09418*, 2024. II-A
- [10] Y. Weng, M. Han, H. He, X. Chang, and B. Zhuang, "Longvlm: Efficient long video understanding via large language models," in *European Conference on Computer Vision*. Springer, 2024, pp. 453–470. II-A
- [11] Z. Shang, Y. Zhu, H. Li, S. Yang, and X. Wu, "Video summarization using denoising diffusion probabilistic model," in *Proceedings of the AAAI Conference on Artificial Intelligence*, vol. 39, no. 7, 2025, pp. 6776–6784. II-B
- [12] H. Yuan, X. Li, T. Zhang, Z. Huang, S. Xu, S. Ji, Y. Tong, L. Qi, J. Feng, and M.-H. Yang, "Sa2va: Marrying sam2 with llava for dense grounded understanding of images and videos," *arXiv preprint arXiv:2501.04001*, 2025. II-C
- [13] S. Munasinghe, H. Gani, W. Zhu, J. Cao, E. Xing, F. S. Khan, and S. Khan, "Videoglamm: A large multimodal model for pixel-level visual grounding in videos," in *Proceedings of the Computer Vision and Pattern Recognition Conference*, 2025, pp. 19 036–19 046. II-C
- [14] Z. Jiang, Z. Han, C. Mao, J. Zhang, Y. Pan, and Y. Liu, "Vace: All-in-one video creation and editing," *arXiv preprint arXiv:2503.07598*, 2025. III-B0d
- [15] T. Wan, A. Wang, B. Ai, B. Wen, C. Mao, C.-W. Xie, D. Chen, F. Yu, H. Zhao, J. Yang *et al.*, "Wan: Open and advanced large-scale video generative models," *arXiv preprint arXiv:2503.20314*, 2025. III-B0d, IV-A
- [16] J. Xiao, A. Yao, Y. Li, and T.-S. Chua, "Can i trust your answer? visually grounded video question answering," in *Proceedings of the IEEE/CVF Conference on Computer Vision and Pattern Recognition*, 2024, pp. 13 204–13 214. IV
- [17] M. Abdin, J. Aneja, H. Behl, S. Bubeck, R. Eldan, S. Gunasekar, M. Harrison, R. J. Hewett, M. Javaheripi, P. Kauffmann *et al.*, "Phi-4 technical report," *arXiv preprint arXiv:2412.08905*, 2024. IV-A
- [18] T. Ren, S. Liu, A. Zeng, J. Lin, K. Li, H. Cao, J. Chen, X. Huang, Y. Chen, F. Yan *et al.*, "Grounded sam: Assembling open-world models for diverse visual tasks," *arXiv preprint arXiv:2401.14159*, 2024. IV-A